The relationship between atmospheric circulation patterns and extreme temperature events in North America

Ryan E. Adams, Kent State University, Dept. of Geography, Corresponding author: radams32@kent.edu

Cameron C. Lee, Kent State University, Dept. of Geography

Erik T. Smith, Kent State University, Dept. of Geography

Scott C. Sheridan, Kent State University, Dept. of Geography

ABSTRACT:

Extreme temperature events (ETEs) pose a significant risk to society, especially vulnerable populations with limited access to shelter and water and those with pre-existing respiratory and cardiovascular ailments. This research examines the relationship of atmospheric circulation with a myriad of metrics related to ETEs to better understand which synoptic-scale circulations are likely to have negative health/thermal comfort outcomes. Daily sea-level pressure (SLP) and 500-hPa geopotential height (z500) data from the North American Regional Reanalysis (NARR) were used to identify circulation patterns over North America. Self-organizing maps were used to partition the variability in circulation patterns over 5 distinct domains covering North America for both variables. Daily 2-m temperature, 2-m dewpoint temperature, and 10-m wind data from the NARR were used to derive five major categories of ETEs based on 95th percentiles: temperature events, apparent temperature events, dew point events, and excess heat and excess cold temperature events. The relationship of circulation pattern frequencies (SOM nodes) leading up to ETEs were assessed using point biserial correlations, accounting for spatial and temporal autocorrelation. The results show that z500 has a stronger association with ETEs than does SLP. A great deal of spatial variability exists in the strength of relationship for many ETE variables with circulation patterns likely due to the local geographical influence (e.g. leeside mountain adiabatic warming and low-level maritime flow). Generally, high extremes are associated with broad ridging and anticyclonic flow and cold extremes are associated with high amplitude trough patterns with low-level flow originating from the continental interior. The use of self-organizing maps presents a unique way of examining the potential for human health risks related ETEs and may be an effective method for statistically downscaling climate model data to assess the potential for ETEs in the future.

This article has been accepted for publication and undergone full peer review but has not been through the copyediting, typesetting, pagination and proofreading process which may lead to differences between this version and the Version of Record. Please cite this article as doi: 10.1002/joc.6610

KEYWORDS: synoptic, atmosphere, extreme weather, humidity, temperature, health

Grant: NOAA Climate Program Office, award number NA17OAR4310159

1. Introduction

Studies on extreme temperature events (ETEs) and their impacts have been increasing steadily, especially within the context of climate change. Many societal sectors are impacted by ETEs, most notable are the impacts on human health. While many studies have investigated the human health response to ETEs, there are limitations to this work. First, given the lack of a consensus on a definition of an ETE (e.g., Perkins and Alexander, 2013; Robinson, 2001), many studies are not directly comparable, especially since ETEs at a location must be defined by both the duration and the intensity. Second, heat events are studied more than cold events (Allen and Sheridan, 2013). While it is well established that heat events are likely to be more critical in terms of impacts moving forward (e.g., Hajat et al., 2014), cold events can also have significant impacts on human health (Lee, 2015).

Of importance in ETE impact research is the topic of human thermal comfort – "a condition of mind that expresses satisfaction with the thermal environment" (Gosling et al., 2014). While this concept is intuitive on the surface, human thermal comfort is in fact quite complex, as it is impacted not only by temperature, but also by dew point (Andersen et al., 2012), wind speed (Steadman et al., 1984), and multivariate surface weather 'situations' (Sheridan et al., 2012a, 2012b; Lee, 2015; Urban and Kysely, 2015; Pena et al., 2015), among other variables. Further, one's thermal comfort is not only impacted by the immediate weather conditions but can be a result of prolonged exposure to oppressive conditions (Lee et al., 2016; Turner et al., 2013), and is also relative to an individual's acclimatization (Donaldson et al., 2003; McMichael et al., 2008).

In addition to thermal comfort, extreme heat events can exacerbate existing cardiovascular, renal and respiratory diseases, leading to mortality (Gronlund et al. 2016). In many parts of the world, extreme heat is compounded by the influence of high dew points. Given the non-linear relationship between dew point and apparent temperature (Steadman 1984), understanding the underlying causal mechanisms of extreme dew point values is also important. From a climate change perspective, increases in atmospheric precipitable water (e.g. Durre et al., 2009) and mean dew point (e.g. Brown

and DeGaetano, 2013) have been observed. Furthermore, many of the warmest years on record have occurred in the past decade. These events make such heat impact studies a relevant area of research.

Exposure to extreme cold has similar effects on human health and thermal comfort. While extreme cold events are largely decreasing in frequency over time, they still occur and present a major hazard to human health. The late January 2019 extreme cold outbreak in North America is a recent example that proved fatal to some, shattering many low temperature records (Glenza 2019). Extreme cold affects human thermal comfort and sometimes leads to increased mortality (e.g. Allen and Lee, 2014), though typically in a more delayed manner in the developed world (Anderson and Bell, 2009), through respiratory ailments, among other causes. Acute-exposure hypothermia is a factor as well (Lim and Duflou, 2008, Spencer and Sheridan, 2015), likely more so in the developing world (e.g., Hashizume et al., 2009). While extreme cold can affect sectors such as agriculture (Aggarwal, 2008), energy (Leahy and Foley, 2012), and infrastructure (Guirguis et al., 2011), the impacts on humans remain the center of attention in many extreme temperature event studies.

Past studies have shown the relationship between extreme heat and sea-level pressure anomalies. High pressure anomalies and flow inhibiting maritime influence are characteristic of dry heat events (Loikith and Broccoli 2013; Horton et al. 2016), while high-pressure anomalies, maritime flow, and positive precipitable water anomalies are characteristic of humid heat events (Tomczyk and Bendnorz 2016). Furthermore, synoptic conditions (e.g. SLP patterns and low-level winds over high terrain) can lead to leeward mountain side enhancement of extreme heat by way of adiabatic warming (Lau and Nath 2012; Lee and Grotjahn 2015; Grotjahn et al. 2016).

Contrastingly, extreme cold is fostered by negative sea-level pressure and upper tropospheric geopotential height anomalies and typically exacerbated when surface winds originate from continental interiors (Tomczyk et al. 2019). The proposed association between Arctic sea-ice loss and extreme cold events in the Northern Hemisphere mid-latitudes (Francis and Skific, 2015) suggests that extreme cold events, with their link to anomalous atmospheric blocking patterns (Räisänen and Ylhaisi, 2011) may continue to occur well into the future, despite an overall decline in frequency (Collins et al., 2013); thus, human health risks related to extreme cold remains a concern, especially among those with preexisting respiratory and cardiovascular ailments.

In the context of health impacts studies, deriving the link between ETEs and atmospheric circulation patterns is useful as the results can increase our understanding of atmospheric regimes

associated with various human health risks. Defining this link is especially important for impact assessments of future climates because it can inform our projection and understanding of future extreme temperature events. Modeling efforts and teleconnection studies have also helped advance our understanding of extreme temperature events and the principal climate patterns associated with them, such as with wintertime temperature extremes in response to the phases of the North Atlantic Oscillation and the Pacific North American pattern teleconnections (Ning and Bradley 2015; 2016). Such efforts can help increase confidence in our understanding of future circulation patterns which will continue affecting human thermal comfort and well-being.

The objective of this research is to examine the relationship between atmospheric circulation and several metrics related to human thermal comfort. There are many definitions of ETEs in the literature and each can be used to study different aspects of thermal comfort; this paper compiles a number of ETE metrics (borrowed and adapted from previous literature) to carry out a comprehensive correlation assessment of each, with two common atmospheric circulation variables. To do so, this paper calculates extreme temperature event metrics for North America (extreme temperatures, extreme dew points, extreme apparent temperatures, excess heat factor, and excess cold factor) and the circulation patterns that are associated with these events. Section two will discuss the data and methods, including the formulation of each metric and atmospheric circulation patterns, and the procedures for investigating the relationship between the two. Section three will discuss a few key results of the extreme weather indicator and circulation pattern relationships. Lastly, section four will conclude with takeaway points, implications, and directions for future research.

2. Data and Methods

a. Reanalysis data

Data from the North American Regional Reanalysis (NARR; Mesinger et al. 2006) were used to identify both the ETEs and circulation patterns over North America. The NARR dataset assimilates data from observations of temperature, moisture, winds and pressure from radiosondes, dropsondes, surface stations, and aircraft. The NARR data has a horizontal resolution of approximately 32-km at the equator, which changes with latitude. Daily mean values of sea-level pressure (SLP), 500-hPa geopotential height (z500), 2-m temperature, 2-m dewpoint, and 10-m winds were retrieved for 5 overlapping regions of North America (Figure 1) for the years 1979 to 2016. The size of these regions was chosen to be slightly larger than typical synoptic-scale features. Five regions were needed, with some overlap, to completely

cover North America. The regions were chosen based on similar synoptic variability, which decreases closer to the tropics; as such, the Gulf domain has a smaller latitudinal extent since variability increases drastically northward into the middle latitudes.

b. Extreme temperature events

Five major categories of ETEs are defined: temperature events, apparent temperature events, dew point events, and excess heat and excess cold temperature events. The first three of these were further broken down into multiple different ETEs, first between high (>95th percentile) and low (<5th percentile) events, and then also further subdivided into absolute events (with percentiles based upon the entire time series), and deseasonalized events (where percentiles are based upon a seasonally-relative curve of the 95th and 5th percentiles). Seasonally-relative curves of each variable were computed by setting each day in a month equal to the monthly mean, and then taking a 31-day centered moving average of this step-like time series, thus smoothing out the discontinuities and representing the extreme ends of each metric relative to the season. Dew point events, in addition to the above-mentioned subdivisions, were also broken down into three different absolute threshold high-humidity events, based upon days with dew points greater than 20°C, 22.5°C or 25°C. The fourth and fifth categories are based upon 2m temperatures, and defined using the methods originally described by Nairn and Fawcett (2014) for heat days/events [excess heat factor – EHF] and modified by Sheridan and Lee (2018) for cold days/events [excess cold factor – ECF]. In brief, excess temperatures incorporate both intensity and duration into the calculation of an event, using a difference between a day's temperature and the 95th (heat) or 5th (cold) percentile of temperatures averaged over a 3-day window. Acclimatization (important in temperature-related mortality research) is also incorporated, as this quantity is then compared to the temperature of the preceding 30 days (for further detail on this method, please see Nairn and Fawcett, 2014, and Sheridan and Lee, 2018). Thus, in total, 19 different ETEs are examined in this research (Table 2), each of which is derived separately for each land-based grid-point in North America.

c. Circulation patterns

To categorize atmospheric flow, circulation patterns (CPs) for SLP and z500 were computed for each region in Figure 1 using self-organizing maps (SOMs; Kohonen 1995, 1989). The SOM approach is an unsupervised neural network algorithm used to classify and reduce data of high dimensionality. The method has garnered a great deal of attention in the discipline of synoptic climatology as a means of

partitioning and visualizing atmospheric patterns (Sheridan and Lee 2011). Since the resultant classification produces a natural organization of patterns across two dimensions (whereby similar patterns are located nearer to each other and dissimilar patterns further apart), a larger number of categories are able to be identified and visualized more easily by comparison to traditional clustering techniques such as k-means. Further, these categories can show the range of circulation patterns characteristic of both dominant and transitional circulation regimes.

Separately for each region and for z500 and SLP, SOMs of different sizes were trained and evaluated to determine which topological structure (horizontal and vertical dimensions) best minimizes intra-pattern variability while maximizing inter-pattern variability. Since finer-scale resolution does not necessarily equate to a better classification (Demuzere et al., 2009), the raw data resolution is reduced by a factor of six, which not only reduces time spent on classification, but also helps to capture circulation features influencing larger-scale temperature events, rather than smaller-scale features with limited geographic coverage. Raw data are then standardized by grid-point and subjected to s-mode principal components analysis (PCA), with the principal components (PCs) with eigenvalues greater than one retained for use in the SOMs. Using MATLAB 2018b and customized code in the Deep Learning Toolbox, SOMs with dimensions between 3x3 and 9x9 were computed on the retained PCs and trained for 500 iterations, with an ordering-phase learning rate of 0.9 and a tuning-phase learning rate of 0.02. Two cluster evaluation metrics were then used to evaluate the performance of each SOM, based upon both the circulation data themselves (internal validation) and partitioning of the ETE data (external validation): the Davies-Bouldin index (DBI; Davies and Bouldin 1979), and the distributed variability skill score (DVSS; Lee 2016). The DBI is a ratio of the inter-pattern scatter to intra-pattern separation, while the DVSS compares the separation and cohesion of each clustering solution against that of 100 randomized clustering solutions of the same size and with the same pattern frequencies. These evaluations were used to weed out poorer SOMs, with final SOM sizes being chosen subjectively from the better performing SOMs according to these metrics. The final SOM sizes whose clustering skill were best are shown in Table 1. Once SOM size was finalized for each variable and region, a final SOM was trained using 10,000 iterations and learning rates of 0.99 and 0.01 for the ordering phase and tuning phase, respectively. Upon completion, each day in the period of record is assigned to the SOM node that the spatial pattern (of SLP or 500z) for that day most closely resembles.

d. Analysis Methods

SOM relationships are evaluated with each ETE metric and region. Nonlinear eta correlation ratios are used to assess the ability of the SOM as a whole (rather than individual CPs within the SOM) to partition ETEs across different CPs at 0 days of lag. Eta correlation (η) is simply the square root of the ratio of the sum of squares between groups/CPs over the total sum of squares in an ANOVA table, and ranges between 0 and 1, with greater values indicating better association. Statistical significance is computed using the F-test statistic in the ANOVA for each grid point. When averaging η across a region, we attempt to estimate the significance via a two-stage analysis. First, we controlled the False Detection Ratio using the method described in Wilks (2016) to account for spatial autocorrelation in testing for field significance [which essentially requires each local test to meet a stricter threshold (lower p-value) to reject the null hypothesis at the α-global=0.05 level]. We then calculated the percentage of the grid points within each region that meet this new stricter threshold, representative of statistical significance at the $p<0.05$ level.

We also test the relationship of 7-day CP frequency anomalies leading up to an extreme temperature event. For each of the final SOM patterns, time series of binary values were created for each SOM node (1 means the pattern occurred, 0 means it did not occur) for the entire study period. Next, 7-day running CP frequencies were computed, subtracting the 1979-2016 circulation pattern climatology from each day of year. These time series were correlated with each of the ETEs by grid point using point-biserial correlations with unpaired t-tests. The point-biserial is similar to the Pearson correlation except that one continuous variable is being measured against a dichotomous variable. These tests were adjusted for both temporal autocorrelation [using the effective sample size adjustment described in Bretherton et al. (1998)] and spatial autocorrelation [by correcting for the false discovery rate (FDR) as discussed in Wilks (2016)]. ETEs are confined to their respective seasons, so circulation frequency time series used for these calculations reflect only the months where these indicators are most prevalent. For example, low absolute apparent temperature events are prevalent during the wintertime months; therefore, only circulation pattern frequencies for DJF months are correlated with DJF indicator time series. Since the values for excess cold events (XCE) are negative (i.e. colder temperatures translate to a more negative XCE), the values were multiplied by (-1) in order to make interpretations of correlations consistent with other ETE variables. In these situations, a positive correlation means that higher circulation pattern frequencies correspond to more negative XCE values [and a greater likelihood of XCE].

3. Results & Discussion

Eta correlations describe the effect size of the SOM classification (as a whole) on ETEs occurring concurrently (at Lag=0) with results generally showing that z500 has a stronger relationship across nearly all domains and ETE variables than does SLP (Table 3a). This is not surprising to find since z500 is a more thermally driven measure than SLP. These results also exhibit the highest degree of association for high temperature events (apparent temperature and regular temperature; absolute and relative) in extreme northern portions of Canada (southern Nunavut) and the Cascades. Contrastingly, the strongest correlations for cold temperature events are found in the Columbia mountains of southwestern Canada, upper Midwest, and interior parts of the eastern U.S. The spatial patterns for excess temperature metrics (heat and cold) are qualitatively like those of the absolute and relative measures of temperature and apparent temperature, albeit with a weaker association. Generally, absolute measures for each variable exhibit stronger relationships with the SOMs than do relative measures of ETEs (Table 3a), especially for northern locations. This could be due to the increased seasonal variability of surface temperatures and dewpoint for higher latitudes. Northern locations experience relatively more CPs than do southern locations throughout the year, and they also experience more anomalous temperature episodes; accordingly, the association of these anomalous temperature events should pose a weaker link than with absolute events, especially considering that CPs are derived using raw (i.e. not seasonally-standardized) variables. The opposite appears true for southern locations. Given the relatively low seasonal variability of temperature here and fewer characteristic CPs throughout the year, relative correlations are typically stronger (in some cases more widespread - such as for anomalous high 2-m temperature and dewpoint events and sea-level pressure for the Gulf region). The percentages of grid points in the nonlinear eta correlation analyses that are statistically significant are found in Table 3b. Nearly all grid points are significant for all ETE variables across each domain and CP, with the exception being absolute dewpoint threshold ETEs. Here, the percentage of significant grid points drops to zero, especially for the highest dewpoint thresholds and for the North and Canadian domains. Dewpoint measures rarely exceed the highest thresholds, especially in the northern locations of North America owing to their distance from warm and moist airmasses, so relative measures of dewpoint can provide more useful information in these cases.

Characteristics of ETEs are spatially and seasonally variable for the period 1979 to 2016. Generally, cold temperature ETEs are more prevalent in northern regions and warm ETEs more prevalent in southern regions. Dewpoint events are nearly exclusively confined to Gulf and southern

portions of the U.S., especially during the boreal summer. There is greater spatial and temporal variability for ETEs when normalized seasonally; here, transitional seasons exhibit both cold and hot ETEs. These seasonally-relative events may be just as important as absolute events given differences in human acclimatization and the ability to adapt in more meteorologically variable seasons.

Individual SOM node correlations reflect the strength of relationship between the 7-day running circulation pattern anomaly and each ETE metric; the strength and significance of the relationships are highly dependent on the domain and the seasonality of the CPs for both z500 and SLP. Generally, z500 correlations are stronger and are confined to fewer nodes of the SOMs. Largely, across each domain, absolute high (JJA) events (2-m temperature, 2-m dewpoint, and apparent temperature) correlate best ($R>0.30$) with broad zonal flow, above average heights, southerly flow, and high-pressure areas; similar to the results found by Loikith and Broccoli (2013). Qian et al. (2016), Chen et al. (2017), and Tomczyk and Bednorz (2019) used anomaly-based approaches of upper-level height structures and found similar upper tropospheric patterns characteristic of lower tropospheric extreme heat, such as positive mid- and upper-level height anomalies. For ridging patterns exhibiting some component of southerly or maritime flow, correlations with extreme dewpoint events and high dewpoint thresholds become stronger, especially for the Gulf of Mexico region. These results align with those of Tomczyk and Bednorz (2016) whose findings show the association of humid events with the inflow of maritime air and high atmospheric precipitable water. Absolute low (DJF) events are most strongly correlated ($R>0.30$) with upper level troughing and strong north to northwesterly flow. Analog circulation patterns of northern Europe have also been associated with extreme cold (Tomczyk et al. 2019).

The z500 SOM and seasonality for the East region is shown in Figure 2. The range of height patterns spans summer dominant CPs in the top left of the SOM and winter dominant CPs in the right and bottom of the SOM. Correspondingly, Figure 3 illustrates the correlation coefficients, by CP, of extreme cold apparent temperature events with the 7-day frequency anomalies of that CP. Patterns 4, 5, and 10 exhibit the strongest positive correlation (dark pink) across the eastern U.S. with widespread statistical significance (all color shading is statistically significant at the 0.05 alpha level); these patterns reflect high amplitude wintertime trough patterns that are characteristic of cold air outbreaks.

Deseasonalized (relative) ETE correlations are more nuanced. Extreme warm/humid relative events are like their absolute event counterparts, except that some patterns with larger amplitude ridging are positively correlated. Cold/Dry events are most correlated with moderate troughing (rather than strong troughing as with the absolute low events). Extreme dewpoint thresholds have little to no

correlation with circulation pattern frequency, except for extreme southern portions of North America and where there is strong southerly flow. Unlike absolute measures, relative extreme warmth associated with adiabatic warming circulation patterns (i.e. z500 ridge and moderate cross-mountain flow) confined to the western Great Plains and interior mountain valleys of northern Canada (leeward side of Columbia, Caribou, and Birch mountains) is more evident, especially for late summer and fall circulation regimes. This may be because such adiabatic warming events on the leeward side of these mountains are common these times of the year given the correct synoptic forcing, but are generally weaker than extreme heat events driven north by advective processes.

4. Conclusions

This study investigates the strength and direction of relationship of extreme temperature events with patterns of SLP and z500 for five regions over North America from 1979 through 2016. The patterns for SLP and z500 were defined using SOMs. The 7-day running circulation pattern anomalies of each SOM were computed and correlated with measures of extreme temperature to gain a better understanding of the precursor synoptic conditions associated with variables related to human thermal comfort. The results of ETEs and CP correlations align with previous literature regarding large-scale circulation with a few noteworthy findings. Correlations for z500 SOMs are stronger than for SLP SOMs, which is expected given our understanding of synoptics and the resulting surface temperature and moisture response. For many ETE variables (temperature, apparent temperature, and excess temperature events), high extremes are most related with broad z500 ridging and anticyclonic flow. Nearly all regions and both z500 and SLP exhibit weak or no significant relationship with dewpoint temperature metrics; some exceptions do exist for the Gulf region and for localities experiencing ridging and low-level, moist flow. The opposite is true for exceptional cold and dry conditions; localities amidst high-amplitude trough patterns and low-level flow originating from inner continental regions are much more strongly related to extreme cold metrics.

The relative ETE measures have weak relationships compared to absolute measures. Of these relationships, the northern locations have the weakest correlations while the southern locations have the highest, due to seasonal variability differences by latitude. Since southerly locations experience less circulation pattern variability, relative correlations are expected to be greater compared to the northern location counterparts. Relative ETE measures do exhibit some stronger relationships, especially with z500 and SLP patterns characteristic of adiabatic warming events. Absolute ETE measures present more robust significance with the overlying circulation, so examining these measures in the context of applied

climate and human thermal comfort studies should pose a more fruitful venture. Further, an examination of circulation pattern and ETE trends can help inform how human health and thermal comfort risks have changed over time and their potential changes for the future. Overall, while the sign of these relationships and the relative correlations among the different ETEs and CPs examined were not surprising, the magnitude of some relationships was stronger than expected (e.g. absolute low apparent temperature event correlations with high amplitude troughing in the eastern U.S. is greater than R≈0.40). Given the extreme and infrequent nature of these ETEs, the strong correlations for many absolute ETE measures with atmospheric circulation may be an effective statistical downscaling method for inferring ETE potential on the local scale. This is a particularly useful finding for impacts research investigating human health and thermal comfort in future climate scenarios and may be a worthwhile avenue for future research.

5. Supporting Information

Supporting figures for the East domain are provided in on-line supplementary material. The SOM for the sea-level pressure is included with its seasonality. Further, grid-based correlation coefficient maps are included for all ETE variables described in Table 2 for both sea-level pressure and 500-hPa geopotential height SOMs. The complete dataset for the circulation patterns and maps for all domains can be found on at http://dx.doi.org/10.17632/6jnr85k4hs.1.

6. Acknowledgments

The authors would like to thank the three anonymous reviewers for their constructive comments in evaluating this manuscript. This work was supported by the NOAA Climate Program Office, award number NA17OAR4310159.

7. References

Aggarwal PK. 2008. Global climate change and Indian agriculture: impacts, adaptation and mitigation. Indian Journal of Agricultural Sciences, 78, 911-919.

Allen MJ, Lee CC. 2014. Investigating high mortality during the cold season: mapping mean weather patterns of temperature and pressure. Theoretical and Applied Climatology 118(3), 419-428. DOI: 10.1007/s00704-013-1075-x.

Allen MJ, Sheridan SC. 2013. High-mortality days during the winter season: comparing meteorological conditions across 5 US cities. International Journal of Biometeorology, 58(2), 217-225.

Anderson BG, Bell ML. 2009. Weather-related mortality how heat, cold, and heat waves affect mortality in the United States. Epidemiology, 20, 205–213.

Andresen J, Hilberg S, Kunkel K. 2012. Historical Climate and Climate Trends in the Midwestern USA. In: U.S. National Climate Assessment Midwest Technical Input Report. J. Winkler, J. Andresen, J. Hatfield, D. Bidwell, and D. Brown, coordinators. Available from the Great Lakes Integrated Sciences and Assessments (GLISA) Center, http://glisa.msu.edu/docs/NCA/MTIT_Historical.pdf.

Åström DO, Forsberg B, Ebi KL, Rocklöv J. 2013. Attributing mortality from extreme temperatures to climate change in Stockholm, Sweden. Nature Climate Change, 3(12), 1050- 1054.

Bentley ML, Stallins JA. 2008. Synoptic evolution of Midwestern US extreme dew point events. International Journal of Climatology 28, 1213-1225, DOI: 10.1002/joc.1626.

Brown PJ, DeGaetano AT. 2013. Trends in US surface humidity, 1930–2010. Journal of Applied Meteorology and Climatology, 52(1), 147-163.

Changnon, D., Sandstrom, M. and Bentley, M., 2006. Midwestern high dew point events 1960- 2000. Physical Geography, 27(6), pp.494-504.

Chen Y, Hu Q, Yang Y, Qian W. 2017. Anomaly based analysis of extreme heat waves in Eastern China during 1981–2013. International Journal of Climatology 37: 509–523.

Collins M, Knutti R, Arblaster J, Dufresne JL, Fichefet T, Friedlingstein P, Gao X, Gutowski WJ, Johns T, Krinner G, Shongwe M, Tebaldi C, Weaver AJ, Wehner M. 2013. Long-term Climate Change: Projections, Commitments and Irreversibility. In: Climate Change 2013: The Physical Science Basis. Contribution of Working Group I to the Fifth Assessment Report of the Intergovernmental Panel on Climate Change [Stocker, T.F., D. Qin, G.-K. Plattner, M. Tignor, S.K. Allen, J. Boschung, A. Nauels, Y. Xia, V. Bex and P.M. Midgley (eds.)]. Cambridge University Press, Cambridge, United Kingdom and New York, NY, USA.

Davies, D. L. and D. Bouldin, 1979: A Cluster Separation Measure. Pattern Analysis and Machine Intelligence, IEEE Transactions on. PAMI-1. 224-227. 10.1109/TPAMI.1979.4766909.

Demuzere, M., Werner, M., van Lipzig, N.P.M. and Roeckner, E. (2009), An analysis of present and future ECHAM5 pressure fields using a classification of circulation patterns. Int. J. Climatol., 29: 1796-1810. doi:10.1002/joc.1821

Donaldson GC, Keatinge WR, Näyhä S. 2003. Changes in summer temperature and heat-related mortality since 1971 in North Carolina, South Finland, and Southeast England. Environmental Research 91, 1-7.

Donat MG, Alexander LV, Yang H, Durre I, Vose R, Caesar J. 2013. Global land-based datasets for monitoring climatic extremes. Bulletin of the American Meteorological Society, 94(7), 997- 1006.

Durre I, Williams CN, Yin X, Vose, R. S. 2009. Radiosonde-based trends in precipitable water over the Northern Hemisphere: An update. Journal of Geophysical Research: Atmospheres, 114(D5).

Francis JA, Skific N. 2015. Evidence linking rapid Arctic Warming to mid-latitude weather patterns. Philosopical Transactions of the Royal Society A, 373, 20140170.

Glenza, J. 2019. Polar vortex 2019: eight dead as Arctic air spreads across Midwest., *The Guardian*, https://www.theguardian.com/us-news/2019/jan/30/polar-vortex-us-weather-latest-temperatures-midwest-east

Gosling SN, Bryce EK, Dixon PG, Gabriel KM, Gosling EY, Hanes JM, Hondula DM, Liang L, Mac Lean PAB, Muthers S, Nascimento ST, Petralli M, Vaos JK, Wanka ER. 2014. A glossary for biometeorology. International Journal of Biometeorology 58(2), 277-308.

Guirguis K, Gershunov A, Schwartz R, Bennett S. 2011. Recent warm and cold daily winter temperature extremes in the Northern Hemisphere. Geophysical Research Letters, 38(17), L17701.

Gronlund, C., A. Zanobetti, G. Wellenius, J. Schwartz, and M. O'Neill. 2016. Vulnerability to renal, heat and respiratory hospitalizations during extreme heat among U.S. elderly. Climate Change. 136, 3-4, 631-645.

Grotjahn R., R. Black, R. Leung, M. Wehner, M. Barlow, M. Bosilovich, and coauthors. 2016. North American extreme temperature events and related large scale meteorological patterns: a review of statistical methods, dynamics, modeling, and trends. Clim Dyn. 46, 1151–1184. doi: 10.1007/s00382-015-2638-6.

Hajat S, Vardoulakis S, Heaviside C, Eggen B. 2014. Climate change effects on human health: projections of temperature-related mortality for the UK during the 2020s, 2050s and 2080s. Journal of Epidemiology and Community Health, doi:10.1136/jech-2013-202449.

Hartmann DL, Klein Tank AMG, Rusticucci M, Alexander LV, Brönnimann S, Charabi Y, Dentener FJ, Dlugokencky EJ, Easterling DR, Kaplan A, Soden BJ, Thorne PW, Wild M Zhai PM. 2013. Observations: Atmosphere and Surface. In: Climate Change 2013: The Physical Science Basis. Contribution of Working Group I to the Fifth Assessment Report of the Intergovernmental Panel on Climate Change [Stocker, T.F., D. Qin, G.-K. Plattner, M. Tignor, S.K. Allen, J. Boschung, A. Nauels, Y. Xia, V. Bex and P.M. Midgley (eds.)]. Cambridge University Press, Cambridge, United Kingdom and New York, NY, USA.

Horton, R. M., J. S. Mankin, C. Lesk, E. Coffel, and C. Raymond, 2016. A review of recent advances in research on extreme heat events. Curr. Clim. Change Rep., 2(4), 242-259.

Kohonen, T., 1995: Self-organizing Maps. Vol. 30, Springer Series in Information Sciences. Berlin: Springer.

Kohonen, T., 1989: Self-Organization and Associative Memory. 3rd ed. Springer-Verlag, 312 pp.

Hashizume M, Wagatsuma Y, Hayashi T, Saha SK, Streatfield K, Yunus M. 2009. The effect of temperature on mortality in rural Bangladesh—a population-based time-series study. 2009. International Journal of Epidemiology, 38(6), 1689-1697.

Lau, N. C. and M. J. Nath. 2012. A model study of heat waves over North America: meteorological aspects and projections for the twenty-first century. J Climate. 25, 4761–4783. doi: 10.1175/JCLI-D-11-00575.1.

Leahy PG, Foley AM. 2012. Wind generation output during cold weather-driven electricity demand peaks in Ireland. Energy, 39(1), 48-53.

Lee, C.C. (2014): The Development of a Gridded Weather Typing Classification Scheme. International Journal of Climatology 35, 641-659. DOI: 10.1002/joc.4010.

Lee CC. 2015. A systematic evaluation of the lagged effects of spatiotemporally relative surface weather types on wintertime cardiovascular-related mortality across 19 US cities. International Journal of Biometeorology 59(11), 1633-1645. DOI: 10.1007/s00484-015-0970- 5.

Lee WK, Lee HA, Lim YH, Park H. 2016. Added effect of heat wave on mortality in Seoul, Korea. International Journal of Biometeorology, 60(5), 719-726.

Lee Y-Y, R. Grotjahn. 2015. California central valley summer heat waves form two ways. J Climate.29, 1201–1217. doi: 10.1175/JCLI-D-15-0270.1.

Lim C, Duflou J. 2008. Hypothermia fatalities in a temperate climate: Sydney, Australia. Pathology, 40(1), 46-51.

Loikith, P. and A. Broccoli, 2013: Comparisons between Observed and model-simulated atmospheric circulation patterns associated with extreme temperature days over North America using CMIP5 historical simulations, J. Climate, 28, 2063-2079.

McMichael AJ, Wilkinson P, Kovats RS, Pattenden S, Hajat S, Armstrong B, Vajanapoom N, Niciu EM, Mahomed H, Kingkeow C, Kosnik M, O'Neill M, Romieu I, Ramirez-Aguilar M, Barreto ML, Gouveia N, Nikiforov B. 2008. International study of temperature, heat and urban mortality: the 'ISOTHURM'project. International Journal of Epidemiology, 37(5), 1121-1131.

Mesinger, F., G. DiMego, E. Kalnay, K. Mitchell, and Coauthors, 2006: North American Regional Reanalysis. Bulletin of the American Meteorological Society, 87, 343–360, doi:10.1175/BAMS-87-3-343.

Ning, L., and R. S. Bradley, 2015: Winter climate extremes over the northeastern United States and southeastern Canada and teleconnections with large-scale modes of climate variability. J. Climate, 28, 2475-2493.

Ning, L., and R. S. Bradley, 2016: NAO and PNA influences on winter temperature and precipitation over the eastern United States in CMIP5 GCMs. Clim. Dyn., 46, 1257-1276

Peña, JC, Aran M, Raso JM, Pérez-Zanón N. 2015. Principal sequence pattern analysis of episodes of excess mortality due to heat in the Barcelona metropolitan area. International Journal of Biometeorology, 59(4), 435-446.

Perkins SE, Alexander LV. 2013. On the Measurement of Heat Waves. Journal of Climate, 26(13), 4500-4517.

Qian W, Wu K, Cheuk-Hin Leung J. 2016. Three-dimensional structure and long-term trend of heat wave events in western Eurasia revealed with an anomaly-based approach. International Journal of Climatology 36: 4315–4326

Räisänen J, Ylhäisi JS. 2011. Cold months in a warming climate. Geophysical Research Letters, 38(22), L22704.

Robinson PJ. 2001. On the definition of a heat wave. Journal of Applied Meteorology, 40(4), 762-775.

Sheridan, C and C. Lee, 2011: The self-organizing map in synoptic climatological research. Progress in Physical Geography: Earth and Environment, 35, 1, 109-119.

Sheridan SC, Lee CC, Allen MJ, Kalkstein LS. 2012a. Future heat vulnerability in California, Part I: projecting future weather types and heat events. Climatic Change, 115(2), 291-309.

Sheridan SC, Allen MJ, Lee CC, Kalkstein LS. 2012b. Future heat vulnerability in California, Part II: projecting future heat-related mortality. Climatic Change, 115(2), 311-326.

Spencer JM, Sheridan SC. 2015. Web-based hypothermia information: a critical assessment of Internet resources and a comparison to peer-reviewed literature. Perspectives in Public Health, 135, 85-91.

Steadman RG. 1984. A universal scale of apparent temperature. Journal of Climate and Applied Meteorology, 23(12), 1674-1687.

Tomczyk, A. M. and Bednorz, E. (2016), Heat waves in Central Europe and their circulation conditions. Int. J. Climatol., 36: 770-782. doi:10.1002/joc.4381.

Tomczyk AM, Bednorz E. 2019. Heat waves in Central Europe and tropospheric anomalies of temperature and geopotential heights. International Journal of Climatology doi: 10.1002/joc.6067

Tomczyk, A. M., E. Bednorz, and A. Sulikowska. 2019. Cold spells in Poland and Germany and their circulation conditions, Int. J. Climatol., 39(10), 4002-4014.

Turner LR, Connell D, Tong, S. 2013. The effect of heat waves on ambulance attendances in Brisbane, Australia. Prehospital and disaster medicine, 28(05), 482-487.

Urban A, Kyselý J. 2015. Application of spatial synoptic classification in evaluating links between heat stress and cardiovascular mortality and morbidity in Prague, Czech Republic. International Journal of Biometeorology, Accepted, in press. DOI: 10.1007/s00484-015-1055- 1.

Wilks, D. S., 2016: ‘‘The stippling shows statistically significant grid points’’: How research results are routinely overstated and overinterpreted, and what to do about it. Bull. Amer. Meteor. Soc., 97, 2263–2273, https://doi.org/10.1175/BAMSD-15-00267.1.

	z500 - **Z**	SLP - **P**
Canada - **C**	5x5	5x5
North - **N**	6x4	5x5
West - **W**	8x3	5x5
Gulf - **G**	6x5	5x4
East - **E**	5x5	6x4

Table 1 – Final SOM sizes (horizontal by vertical) for each variable and domain.

Variable	High/Low	Type	Abb.	Description
Temperature	high	Absolute	THA	2m temperatures >95th percentile
		Deseasonalized	THD	2m temperatures seasonal curve of the >95th percentile
	low	Absolute	TLA	2m temperatures <5th percentile
		Deseasonalized	TLD	2m temperatures seasonal curve of the <5th percentile
Apparent Temperature	high	Absolute	AHA	2m apparent temperatures >95th percentile
		Deseasonalized	AHD	2m apparent temperatures seasonal curve of the >95th percentile
	low	Absolute	ALA	2m apparent temperatures <5th percentile
		Deseasonalized	ALD	2m apparent temperatures seasonal curve of the <5th percentile
Dewpoints	high	Absolute	DHA	2m dewpoints >95th percentile
		Deseasonalized	DHD	2m dewpoints seasonal curve of the >95th percentile
	low	Absolute	DLA	2m dewpoints <5th percentile
		Deseasonalized	DLD	2m dewpoints seasonal curve of the <5th percentile
	20		D20	2m dewpoints >20C
	22.5		D22.5	2m dewpoints >22.5C
	25		D25	2m dewpoints >25C
Excess Temperature	heat	day	XHD	Excess Heat Day (Nairn & Fawcett, 2014)
		event	XHE	Excess Heat Event (Nairn & Fawcett, 2014)
	cold	day	XCD	Excess Cold Day (Sheridan & Lee, 2018)
		event	XCE	Excess Cold Event (Sheridan & Lee, 2018)

Table 2 – All ETE metrics used in the study, including the base variable used to calculate them, their abbreviations, and a short description of each.

ETE Variable	CZ	CP	EZ	EP	GZ	GP	NZ	NP	WZ	WP	AVG
THA	0.446	0.206	0.416	0.215	0.372	0.240	0.434	0.251	0.453	0.286	0.332
THD	0.195	0.130	0.174	0.135	0.168	0.123	0.168	0.127	0.167	0.141	0.153
TLA	0.398	0.219	0.408	0.350	0.352	0.332	0.359	0.278	0.350	0.348	0.339
TLD	0.166	0.125	0.177	0.177	0.167	0.162	0.194	0.172	0.174	0.193	0.171
AHA	0.455	0.203	0.421	0.210	0.381	0.231	0.443	0.254	0.466	0.286	0.335
AHD	0.196	0.125	0.169	0.121	0.165	0.114	0.166	0.121	0.167	0.134	0.148
ALA	0.406	0.225	0.415	0.351	0.352	0.319	0.358	0.279	0.349	0.343	0.340
ALD	0.166	0.135	0.182	0.178	0.168	0.161	0.190	0.171	0.174	0.195	0.172
DHA	0.445	0.211	0.403	0.211	0.341	0.195	0.440	0.250	0.382	0.246	0.312
DHD	0.194	0.142	0.178	0.144	0.138	0.107	0.152	0.122	0.137	0.133	0.145
DLA	0.401	0.221	0.404	0.347	0.263	0.281	0.350	0.278	0.310	0.329	0.318
DLD	0.162	0.131	0.171	0.175	0.113	0.144	0.179	0.166	0.136	0.173	0.155
D20	0.118	0.078	0.392	0.223	0.524	0.342	0.064	0.056	0.256	0.196	0.225
D22.5	0.054	0.052	0.263	0.151	0.462	0.276	0.049	0.047	0.193	0.145	0.169
D25	0.038	0.046	0.098	0.068	0.164	0.094	0.040	0.045	0.074	0.064	0.073
XCE	0.144	0.095	0.158	0.146	0.142	0.145	0.161	0.112	0.143	0.149	0.139
XCD	0.345	0.191	0.357	0.299	0.304	0.307	0.320	0.240	0.297	0.309	0.297
XHE	0.172	0.082	0.144	0.095	0.144	0.105	0.166	0.103	0.172	0.114	0.130
XHD	0.413	0.176	0.382	0.194	0.359	0.231	0.411	0.233	0.425	0.261	0.309
AVG	0.259	0.147	0.279	0.199	0.267	0.206	0.245	0.174	0.254	0.213	0.224

Table 3a – Average nonlinear eta correlations, 0 day lag, between each ETE variable (rows) and each circulation pattern classification (columns) for each region (darker greens indicate stronger correlations). The names of the circulation classifications are given by two letters, the first referring to the domain and the second referring to the variable (e.g. 'CZ' are the correlations for the z500 SOM for the Canada domain). Row and column averages are also provided.

ETE Variable	CZ	CP	EZ	EP	GZ	GP	NZ	NP	WZ	WP
THA	100%	100%	100%	100%	100%	100%	100%	100%	100%	100%
THD	100%	100%	100%	100%	100%	100%	100%	100%	100%	100%
TLA	100%	100%	100%	100%	100%	100%	100%	100%	100%	100%
TLD	100%	100%	100%	100%	100%	100%	100%	100%	100%	100%
AHA	100%	100%	100%	100%	100%	100%	100%	100%	100%	100%
AHD	100%	100%	100%	100%	100%	100%	100%	100%	100%	100%
ALA	100%	100%	100%	100%	100%	100%	100%	100%	100%	100%
ALD	100%	100%	100%	100%	100%	100%	100%	100%	100%	100%
DHA	100%	100%	100%	100%	100%	100%	100%	100%	100%	100%
DHD	100%	100%	100%	100%	100%	99%	100%	100%	100%	100%
DLA	100%	100%	100%	100%	100%	100%	100%	100%	100%	100%
DLD	100%	100%	100%	100%	98%	100%	100%	100%	100%	100%
D20	85%	79%	95%	95%	89%	88%	38%	30%	82%	79%
D22.5	26%	33%	75%	75%	91%	93%	24%	0%	78%	71%
D25	0%	9%	58%	52%	76%	69%	0%	0%	38%	34%
XCE	100%	100%	100%	100%	100%	100%	100%	100%	100%	100%
XCD	100%	100%	100%	100%	100%	100%	100%	100%	100%	100%
XHE	100%	100%	100%	100%	100%	100%	100%	100%	100%	100%
XHD	100%	100%	100%	100%	100%	100%	100%	100%	100%	100%

Table 3b – Percentage of locally statistically significant ($p<0.05$) eta correlations between each ETE variable (rows) and each circulation pattern classification and region (columns).

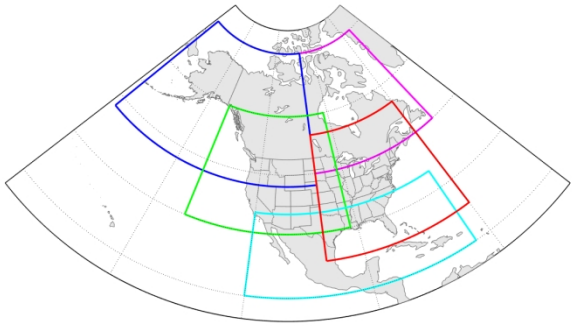

Figure 1 – Regional partitions used in the study. The names of the domains are as follows: Canada (magenta), North (blue), West (green), Gulf (cyan), and East (red).

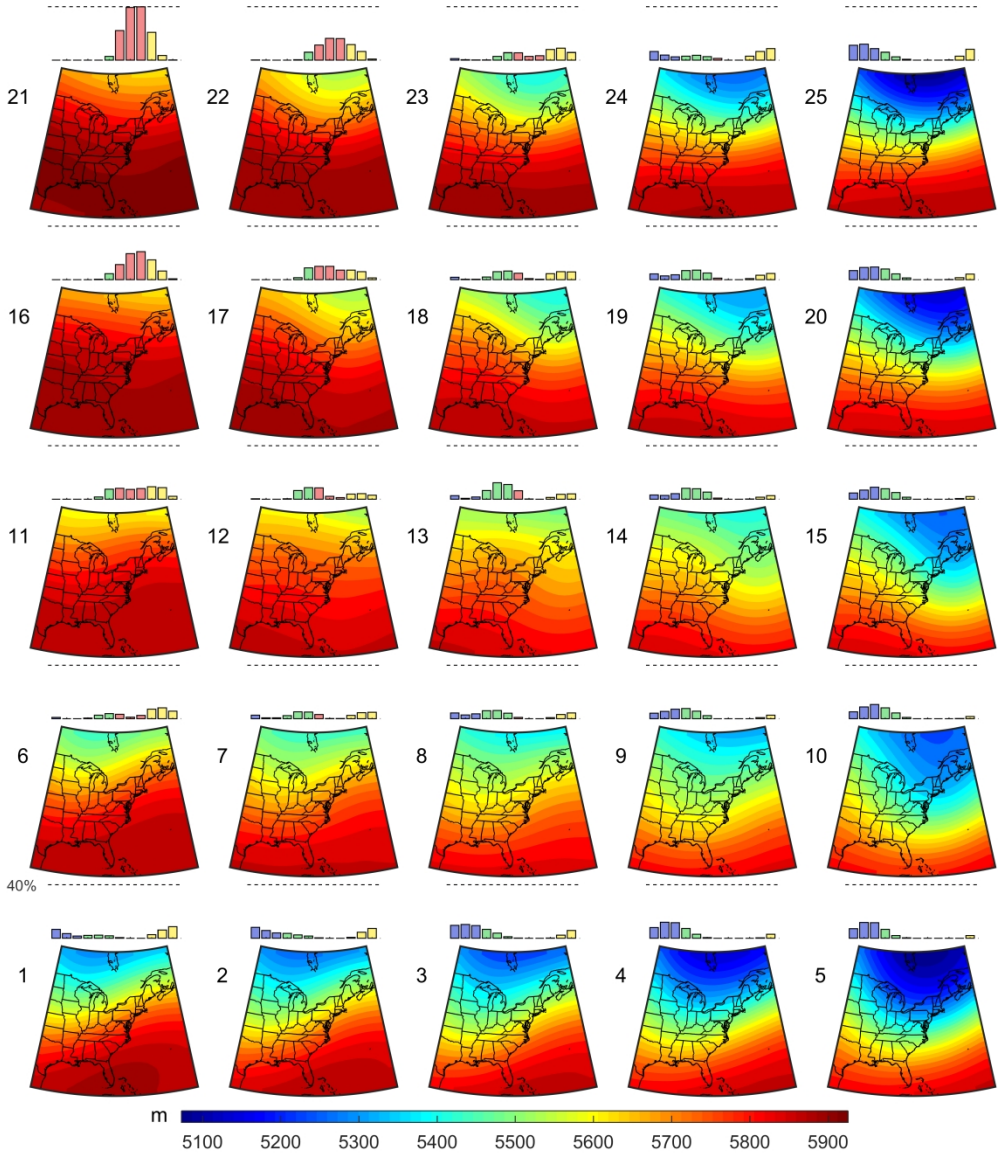

Figure 2 – SOM patterns and seasonality (z500) for the East U.S. domain. Seasonality of each respective pattern is shown in the corresponding bar chart starting with the month of December on the left and colored according to meteorological seasons.

190x221mm (600 x 600 DPI)

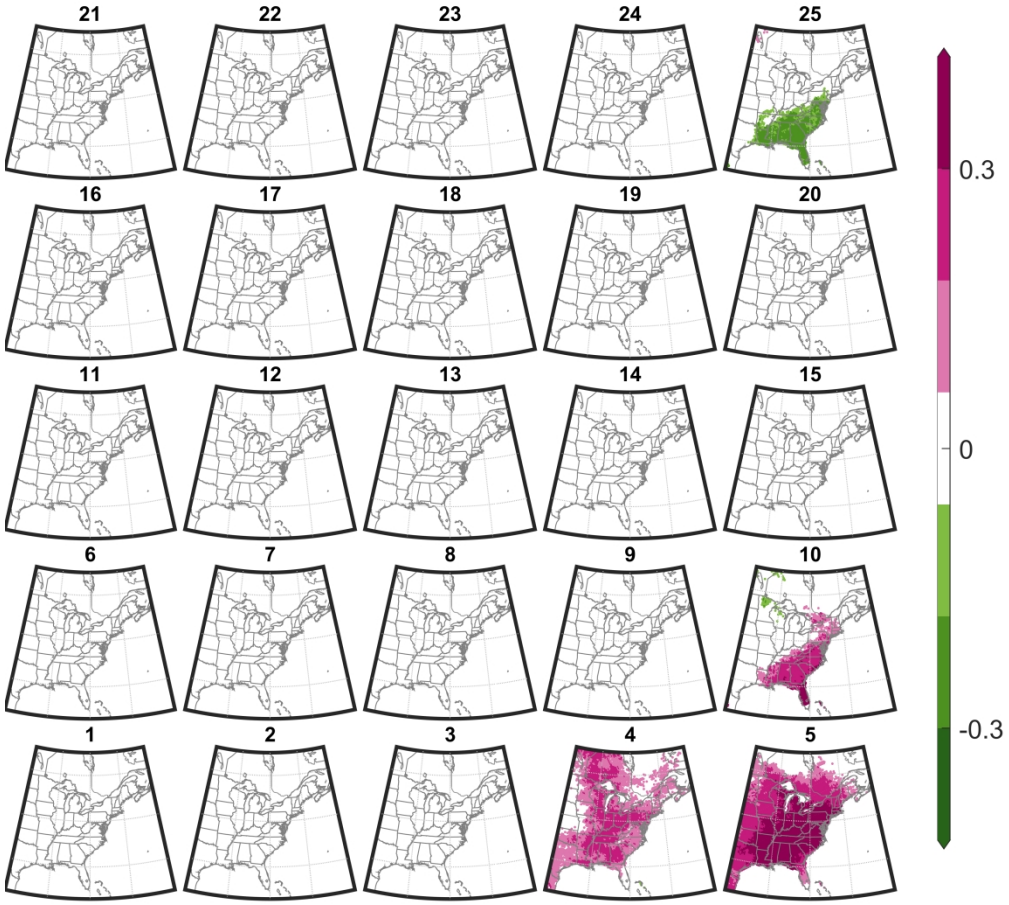

Figure 3 – Grid based correlation coefficients for absolute low apparent temperature events and z500 for the East U.S. domain. Positive values mean that absolute low apparent temperature events are associated with increased frequency of that circulation pattern over the previous 7 days. Shaded areas are statistically significant at the 0.05 alpha level.